



# Study on the seepage characteristics of deep buried tunnels under variable high-pressure water heads

Yingchao Wang<sup>1,2</sup> · Zhaoyang Li<sup>1,2</sup> · Hongwen Jing<sup>1,2</sup> · Yabo Li<sup>1,2</sup> · Mitian Wang<sup>1,2</sup>

Received: 13 February 2020 / Accepted: 26 September 2020 / Published online: 10 October 2020  
© Springer-Verlag GmbH Germany, part of Springer Nature 2020

## Abstract

Well-connected seepage channels are the key components of tunnel water inrush. To study the trends of the pore water pressure in the rock mass in a seepage channel, the physical experiment and corresponding numerical model were established. First, in the seepage experiment under excavation disturbance, the propagation rate of the high-pressure water source and the growth rate of the pore water pressure in the rock mass were analyzed by considering the different water pressures. Second, under the same model size, parameters, and working conditions, the finite element method was used to simulate the seepage process of water in the rock mass. From the microlevel, the evolution process of the pore water pressure isosurface was obtained. The results showed that the pressure water head is positively correlated with the pore water pressure in the rock mass, which displays multiple approximate relationships. Moreover, when the water pressure is high, excavation disturbance can significantly increase the pore water pressure in the rock mass. The disturbance caused by the first excavation is larger than the subsequent excavations. In addition, the research results were compared with previous results. Reasonable agreements that would provide a reference for the conditions of high water-pressure disasters in deep buried tunnel construction were obtained.

**Keywords** Water inrush · High-pressure water head · Excavation disturbance · Seepage characteristics

## Introduction

The construction of deep buried tunnels has been a long-standing challenge (Wang et al. 2019a, b). Under the combined action of high ground stress and high-pressure water, disasters such as rock burst and water inrush frequently occur, which have immeasurable consequences for safety, economic, and the ecological environment (Wu et al. 2019a). High-pressure water inrush disasters are characterized by strong explosiveness and large water inflow. Because surface water and groundwater are interconnected, water inrush has a relatively high impact on the lives of residents (Farhadian and Nikvar-Hassani 2019; Golian et al. 2018). Fortunately, many

scholars have carried out extensive research on effectively preventing the occurrence of water inrush disasters. Significant results have been achieved in the classification of disaster patterns (Lu 2017), determination of influencing factors (Li et al. 2017; Li and Wu 2019), and risk assessment of tunnel water inrush (Wang et al. 2016, 2017, 2019c, d; Li et al. 2020).

The formation conditions of water inrush and its influencing factors reveal that geological conditions are internal factors, and engineering disturbances are external factors (Zhang et al. 2019; Chen et al. 2020). Water inrush is fundamentally caused by the external excavation disturbances breaking the initial equilibrium state of the internal groundwater system. Previous studies showed that high-permeability pressure and high ground stress under strong unloading conditions are the main factors leading to water inrush disasters (Yang et al. 2019). Under the action of high-pressure water, hydraulic fracturing often occurs in the rock mass. The essence of hydraulic fracturing is the expansion of intermittent joint cracks in the rock mass under the action of a high-pressure water head, which would further widen after penetration (Bukowski 2011; Jiang et al. 2020). The geological defects in the rock mass provide a more convenient method for

---

✉ Yingchao Wang  
wych12345678@126.com

<sup>1</sup> State Key Laboratory for Geomechanics and Deep Underground Engineering, China University of Mining and Technology, Xuzhou 221116, Jiangsu, China

<sup>2</sup> School of Mechanics & Civil Engineering, China University of Mining and Technology, Xuzhou 221116, Jiangsu, China

seepage. To simulate various types of geological defects more accurately, Zhou et al. (2015) developed new fluid-solid coupling similar materials. This material can better simulate the state of rock eroded by water flow. Many factors including porous media seepage (Zhang et al. 2020) and pore water pressure distribution (Li et al. 2018b) have been considered by scholars.

Numerical simulation can analyze the seepage process from the micro-level, which can be accurate down to a certain particle or unit (Li et al. 2016). This advantage is unmatched by physical experiments. As a complementary research method, numerical simulation can be divided into two categories: finite element methods and discrete element methods. Many software such as PFC (Wang et al. 2019e), FLUENT (Zhao et al. 2018; Wu et al. 2019b), and FLAC 3D (Pan et al. 2019), have been widely used. During the experiment, the multifield information fusion technology was also used to summarize the evolution of water inrush (Zhang et al. 2018). However, limited by technical conditions, it was difficult to simultaneously apply high ground stress and high water pressure to simulate deep buried tunnels.

Accurately identifying the patterns of seepage in the rock mass is a prerequisite for the effective treatment of tunnel water inrush (Li et al. 2018a). The purpose of this study is to explore the seepage evolution patterns of water in rock mass in a deep buried tunnel under the disturbance of excavation. The pressure water head was used as an independent variable in the experiments, and the pore water pressures at the monitoring points can be obtained. The material parameters and excavation conditions were set according to the field data of the Qiyueshan Tunnel. Moreover, the finite element software, MIDAS/GTS NX, was used to construct the seepage-stress coupling calculation model. According to the principle of effective stress, stress analysis and seepage analysis were alternately performed. After each step of excavation, the seepage calculation was executed once. Finally, the experiment and simulation results were compared and then verified with previous studies.

## Experimental device and research method

### Engineering background

The material parameters and experimental ideas originated from the water inrush disasters caused by the filled karst structures in the Qiyueshan Tunnel. The surrounding rock of the DK363 + 966~DK364 + 218 section of the Qiyueshan Tunnel is grade IV, mainly limestone. The burial depth of this section is between 500 and 580 m. The underground filled karst structures are developed, mostly karst caves and karst pipes (Zhu 2010). The fracture of the fillings in karst structures caused by the infiltration of the high-pressure water source,

and external excavation disturbances led to the water inrush disaster. Compared with previous experiments, this experiment could better apply to the extreme confining pressure and pressure water source faced by deep buried tunnels. This experiment can also monitor the whole seepage process to study the evolution of the pore water pressure in the rock mass with time.

### Experimental device

In this study, a physical experimental system for the mechanism of water inrush in deep buried and long tunnels (Jing et al. 2019) independently developed was adopted. The experimental system is mainly used to explore the processes of stress, deformation, and failure of rock mass under the combined action of complex stress, water pressure, and the influence of tunnel excavation in deep buried tunnels. The experimental device (Jing et al. 2019) includes a high-pressure nitrogen tank group, a gas-liquid composite constant-pressure water tank, a main loading-bearing structure, an in situ stress loading system, a model push-in position device, and a servo hydraulic control system.

The constant pressure of the pressurized water source is mainly maintained by the combined action of the high-pressure nitrogen tank group and the constant-pressure water tank. The inlet pipe at the upper part of the water tank is connected to the nitrogen tank group, and the outlet pipe at the lower part of the water tank is connected to the water inlet in the middle of the model body. The model body is made by pouring different materials. During the casting of the model body, the inlet of the water inlet pipe needs to be buried in advance to simulate the high-pressure water source in the rock mass. The servo hydraulic control system is mainly composed of a servo oil source and a control cabinet. The system pressure is 31.5 MPa, the static pressure stabilization accuracy is  $\pm 0.5\%$ , and the dynamic pressure stabilization accuracy is  $\pm 2.0\%$ . It should be noted that the loading value collected and displayed by the hydraulic control system is the system oil pressure  $\sigma_s$ . Equation 1 provides the conversion relationship between the actual load value  $\sigma_d$  and the oil pressure  $\sigma_s$  according to the model size and load calibrations:

$$\sigma_d = \sigma_s / 3.55 \quad (1)$$

### Material parameters

Two fluid-solid coupling similar materials were developed to simulate the tunnel surrounding rock and karst filling of the Qiyueshan Tunnel site. In the experiments, the following similar ratios were used: the geometric similarity ratio  $C_l = 10$ , the bulk density similarity ratio  $C_\gamma = 1$ , the permeability coefficient similarity ratio  $C_k = 3$ , the dimensionless constant similarity

ratio  $C_\varepsilon = C_\varphi = C_\mu = 1$ , and the stress and elastic modulus similarity ratio  $C_\sigma = C_E = C_\gamma \cdot C_l = 10$ . After the on-site sampling, model making, uniaxial compression testing, Brazilian split testing, different angle shearing testing, and permeability testing, the material parameters of the surrounding rock and karst filling material could be determined. Then, cement, sand, and water were selected to prepare the similar materials for the surrounding rock. Among them, sand was used as aggregate, and cement was used as cementing material. The material properties were changed by adjusting the proportion of water. The same controlled variable method was used to prepare similar materials for the karst filling by selecting clay, sand, and talcum. Talc was used as a variable. Related physical and mechanical tests were also performed to obtain various mechanical parameters of the similar materials. The results are shown in Table 1 (Wu 2017; Zhou et al. 2015). The parameters in Table 1 are the average of the range obtained by experiments. The manufacturing process of similar materials for surrounding rock and the manufacturing process of similar materials for karst filling are shown in Figs. 1 and 2, respectively.

## Experimental process

The pore water pressure is easy to monitor and can effectively express the seepage strength. In this experiment, WMS-51 water pressure sensors were used to obtain the value of pore water pressure. Each monitoring point was separated by 0.1 m, for a total of 5 monitoring points. The first monitoring point was 0.1 m away from the confined water source. All the monitoring points are arranged along the longitudinal center-line of the model. The model after pouring is shown in Fig. 3. Excavation was performed by a drilling rig. Through data monitoring, after the initial seepage was stabilized, the excavation was carried out step by step every 5 min and 5 cm for each excavation. Data collection was carried out at the same time. The experiment was stopped when the confined water spouted on a large scale.

Vertical and horizontal loads were applied to simulate the original rock stress. Based on the average burial depth and rock weight of the selected tunnel section, the self-weight stress of the surrounding rock was calculated to be 14.15 MPa. According to the rock mass Poisson's ratio of 0.3 and Eq. 2, the stress of the surrounding rock in the horizontal direction was approximately 6.06 MPa. It was determined from the similarity ratio and Eq. 1 that a vertical pressure of 1.415 MPa needed to be applied to the model, and the oil pressure was displayed as 5 MPa. A pressure of 0.61 MPa was needed to be applied horizontally, and the corresponding oil pressure was shown as 2.17 MPa. The confined water head was used as the control variable, and the experiments were performed at 0.1 MPa, 0.2 MPa, and 0.4 MPa. A total of three sets of models were made in this experiment, and tests 1, 2, and 3 were executed on these models during the experiment. These tests represented the water pressures of 0.1 MPa, 0.2 MPa, and 0.4 MPa, respectively. The initial seepage stability and experimental excavation are shown in Fig. 4. The longest excavation distance in test 1 was 22 cm, and water inrush occurred during the fifth excavation.

$$\sigma_{horizontal} = \frac{\mu}{1-\mu} \sigma_{vertical} \quad (2)$$

## Analysis of the experimental results

### Analysis of pore water pressure in the initial seepage stable stage

In actual engineering, the osmotic pressure in the tunnel rock mass before excavation is in a balanced state. After opening the water valve, it took 20 min for each model to reach the initial seepage stability. Since the filling material had better resistance to seepage, whether the seepage had reached stability could only be judged by monitoring data. Within the

**Table 1** Parameters of surrounding rock, karst filling, and similar materials (Wu 2017; Zhou et al. 2015)

	Bulk density/ kN/m <sup>3</sup>	Uniaxial compressive strength/MPa	Elastic modulus/ GPa	Tensile strength/ MPa	Cohesion/ MPa	Internal friction angle/°	Permeability coefficient/cm/s	Poisson ratio
Surrounding rock	26.2	53.12	4.04	4.03	5.377	24.23	$2.017 \times 10^{-6}$	0.3
Similar material	26.2	5.312	0.4	0.4	0.54	24.23	$0.672 \times 10^{-6}$	0.3
Mass ratio	Cement/sand/water = 4:4:1							
Karst filling	17.66	13	1.0	0.12	0.2	17	$10^{-4}$	0.25
Similar material	17.66	1.3	0.1	0.012	0.02	17	$0.333 \times 10^{-5}$	0.25
Mass ratio	Clay/Sand/Talcum = 5:5:1							

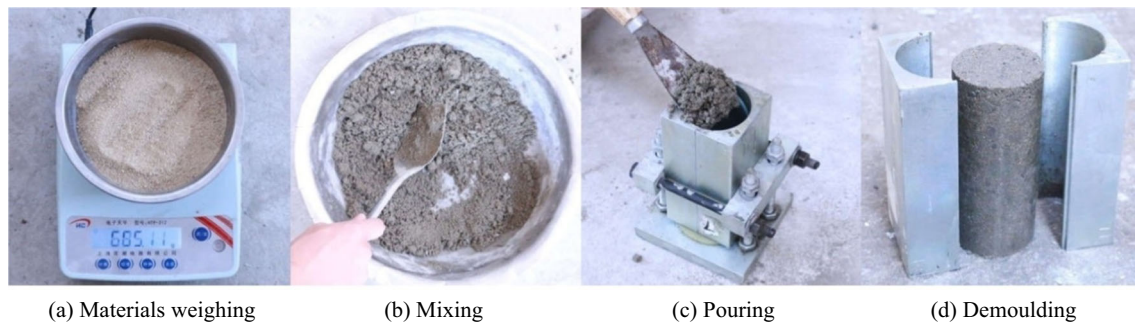


**Fig. 1** Manufacturing process of similar materials for surrounding rock. **a** Material weighing. **b** Mixing. **c** Pouring. **d** Demoulding

5 min before the first excavation, there was no sign of water leakage on the surface of the filling material, as shown in Fig. 4. With the loading of different water pressures, the seepage of pore water needed different times to transfer to the other end of the model and reach a stable state. As seen from Table 2, when the seepage flow was stable, the values of pore water pressure at the same monitoring point in different tests were approximately doubled with increasing test number.

#### Variation in pore water pressure and hydraulic gradient in the initial stable stage

The pore water pressure and its increasing rate curves at each monitoring point in the seepage stage under different water pressure conditions are shown in Fig. 5. Among them, the value of test 3 is the largest, and the value of test 1 is the smallest. The three curves always maintain a stable spacing. The change trends are almost the same, indicating that the evolution of the pore water pressure in the tunnel rock mass is almost the same. In other words, in the absence of excavation disturbance, the pressure of the confined water source has little effect on the change of the pore water pressure in the tunnel rock mass. Under the condition that the internal structure is complete, the rock mass has a good resistance to hydraulic erosion.

The increase rate of the pore water pressure can be divided into two cases. The increase rate of the pore water pressure at

the first three monitoring points is in a decreasing state. Since monitoring points 4 and 5 are far from the confined water pressure, the pore water pressure increasing rate increases first and then decreases, mainly because of the increase in the seepage distance. Expansion seepage occurs at the end far from the confined water source and requires a process of energy accumulation. Here, Eq. 3 is used to calculate the increase rate of the pore water pressure in the seepage stage:

$$v = \frac{P_{n+1} - P_n}{\Delta t} \quad (3)$$

where  $v$  is the change rate of the pore water pressure, MPa/s.  $P_n$  is the pore water pressure at moment  $n$ , MPa.  $P_{n+1}$  is the pore water pressure at moment  $n + 1$ , MPa.  $\Delta t$  is the time interval, s.

Since the monitoring points are equally spaced, the hydraulic gradient of the adjacent monitoring points is calculated by Eq. 4:

$$J = \frac{h_n - h_{n+1}}{\Delta l} \quad (4)$$

where  $h$  represents the confined water head, which is replaced by the pore water pressure. Here, a 1 MPa pore water pressure equal to a 100-m high confined water head is used for conversion, and  $\Delta l$  is the distance between adjacent points.

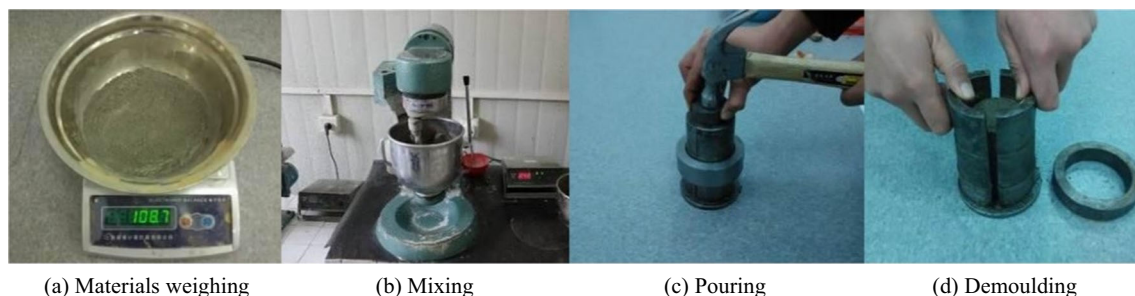
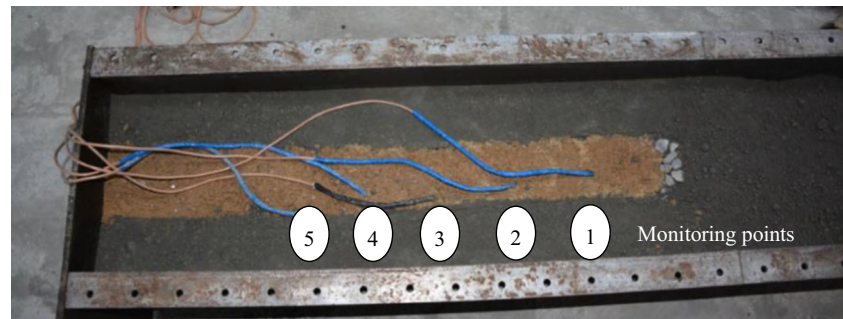


**Fig. 2** Manufacturing process of similar materials for karst filling. **a** Material weighing. **b** Mixing. **c** Pouring. **d** Demoulding

Fig. 3 Casted model



Special time points including 5 s, 100 s, and 500 s are taken to draw the curve of the hydraulic gradient change, as shown in Fig. 6. The hydraulic gradients of the three sets of tests gradually decrease as they move away from the confined water source. Taking  $t = 100$  s as an example, within the range of 0–0.1 m from the confined water source, the hydraulic gradients of tests 1, 2, and 3 are 35.25, 80.6, and 142.55, respectively. Within the range of 0.4–0.5 m from the confined source, the hydraulic gradients decreased to 5.97, 10.66, and 24.52. They decreased by 83.06%, 86.77%, and 82.8%, respectively. The confined water pressures of the three tests are different, and the difference is large, where the hydraulic gradient of test 3 is the largest and that of test 1 is the smallest. It can be seen from Fig. 6 that the hydraulic gradient value of test 3 increases from 2 to 234 at 5 s and from 42 to 77 at 500 s, with a significantly reduced range. As time passes, the hydraulic gradient value on the centerline of the tunnel rock mass becomes increasingly concentrated. This is because the hydraulic gradient distribution becomes more uniform as the pore water pressure becomes linear.

#### Variation in the pore water pressure during tunnel excavation

In tests 1, 2, and 3, water inrush occurs at 22, 17, and 12 cm of excavation, respectively. From the monitoring point 5 to monitoring point 1, the degree of disturbance by the excavation is reduced in turn. The pore water pressure difference at monitoring point 5 before and after excavation is shown in Table 3. The symbol “–” in the table represents the occurrence of water

inrush. As seen from Table 3, with increasing the water pressure, the change of the pore water pressure at the fixed monitoring point caused by excavation. The seepage stability under high water pressure is more affected by excavation disturbances. According to the excavation length of different tests, with increasing pressure of the confined water source, the thickness needed to resist the confined water pressure becomes increasingly larger.

#### Comparative analysis of engineering results and experimental results

On January 15, 2007, during the digging of the Qiyueshan Tunnel to DK364 + 218, a small-scale water inrush disaster was caused because of advanced geological drilling revealing the filled karst structure. The water inrush phenomena in the physical experiment are shown in Fig. 7. The excavation simulation in the experiment is realized by rig propulsion. This is similar to the water inrush caused by advanced geological drilling in actual engineering. Because there are hidden high-pressure water sources in front, the filled rock mass softens under the action of seepage. This causes less thrust to be required by the rig. The mud content in both actual engineering and experimental exudates decreases with time, mainly because in the early stage of water inrush, the water flow brings out filling particles. In the later period, the wider surge channel is formed, so the protrusions are mainly clear water. This further verifies the formation process of the seepage channel.

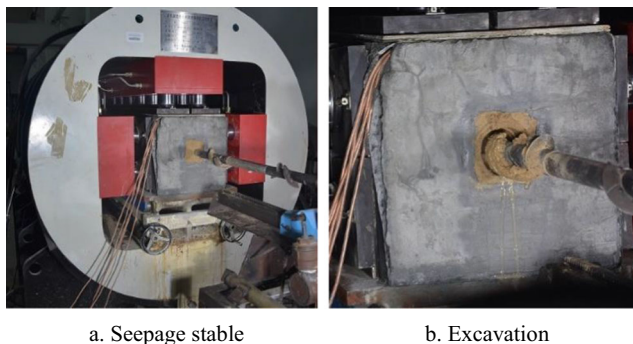
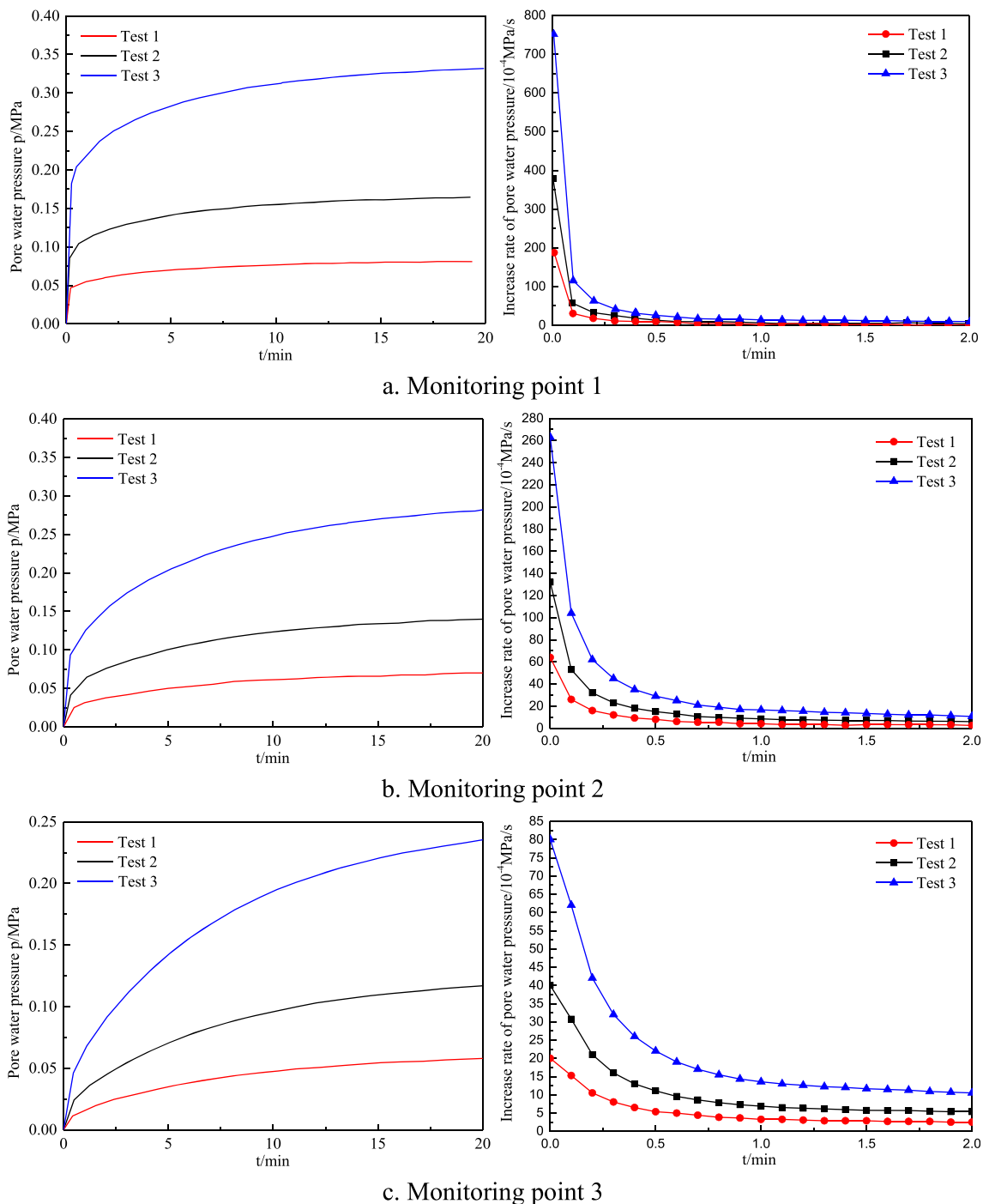


Fig. 4 Excavation and water inrush. a Seepage stable. b Excavation

**Table 2** Pore water pressure values at each monitoring point in the seepage stable stage

The number of tests	The pore water pressure value/MPa				
	Point 1	Point 2	Point 3	Point 4	Point 5
Test 1	0.082	0.069	0.058	0.047	0.036
Test 2	0.166	0.141	0.117	0.095	0.074
Test 3	0.332	0.281	0.235	0.191	0.149



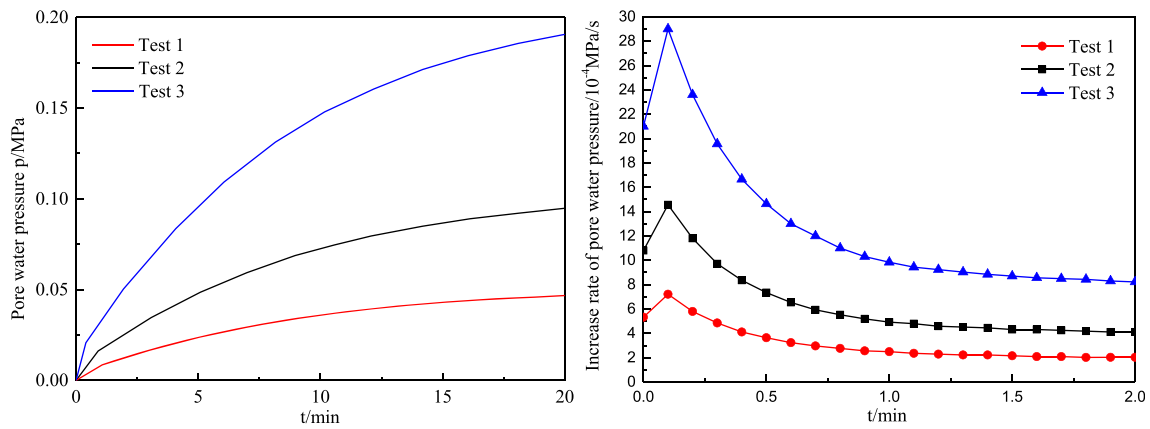
**Fig. 5** Pore water pressure and its increasing rate. **a** Monitoring point 1. **b** Monitoring point 2. **c** Monitoring point 3. **d** Monitoring point 4. **e** Monitoring point 5

## Numerical simulation and result analysis

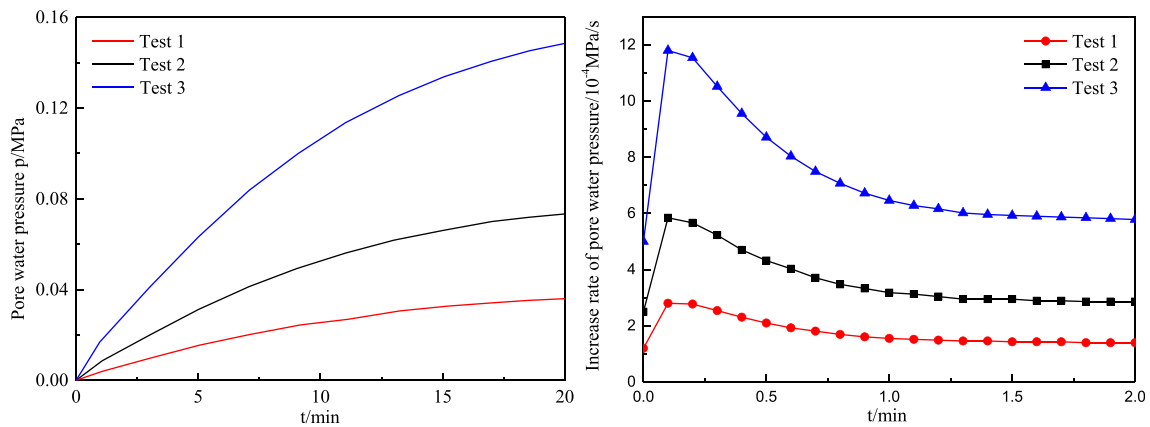
### Numerical model

This model simulated the seepage-stress coupling through the finite element method. It could be used to simulate tunnel excavation and groundwater seepage in high geo-stress and high water pressure conditions. The setting of the size,

excavation process, vertical and horizontal loads, layout of monitoring points, and material parameters of the numerical model is consistent with the experiments. The material parameters were set according to Table 1. The model is shown in Fig. 8. The division of the solid mesh was realized by the software's own hybrid mesh generator. The surrounding rock entities were divided according to the side length of 2 cm, and the tunnel excavation entities were divided according to 1 cm.



d. Monitoring point 4



e. Monitoring point 5

Fig. 5 continued.

The M-C model is used as a failure criterion for two materials. The rock seepage failure can be divided into tensile failure and shear failure. When the rock integrity is good, the seepage failure should be dominated by tensile failure. When there are many cracks on the surface of the rock mass and the integrity is poor, the original cracks would continue to expand under the action of water pressure, resulting in shear failure of the rock mass. The surrounding rock on site is classified as level IV, and the integrity is classified at the

poor level. The filling is eroded by groundwater all year round, which makes the rock mass integrity worse. Therefore, the selection of the M-C constitutive model is appropriate. Unsaturated rock mass refers to a rock mass whose inner pores are not filled with water, which is very common in nature. The model in the experiment is classified as an unsaturated rock mass. Therefore, in the calculation of the seepage, the unsaturated characteristics should be considered. The Van Genuchten function is currently the

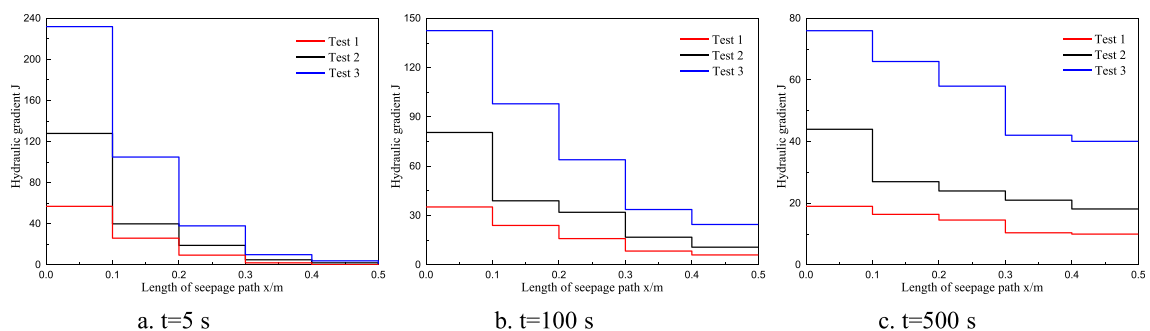


Fig. 6 Variation of hydraulic gradient of pore water pressure. a  $t = 5$  s. b  $t = 100$  s. c  $t = 500$  s

**Table 3** The change of pore water pressure difference at monitoring point 5 before and after excavation

The number of tests	The change of pore water pressure at monitoring point 5/MPa				
	1st	2nd	3rd	4th	5th
Test 1	0	0	0.003	0.004	0.009
Test 2	0.0048	0.0101	0.0151	0.095	–
Test 3	0.03	0.04	0.078	–	–

most effective unsaturated seepage function for rock and soil, as confirmed in many previous studies. This function considers the effect of the viscous force of the water itself on the seepage, ensuring that the parameters of the rock and soil body would change with the changing internal water content.

Static constraints were applied around the model to facilitate computational convergence. The right end of the model was set as the node pressure water head, and the excavation side was set as the seepage surface. The node pressure head was changed to simulate the confined water pressure changing in the experiments. The seepage-stress coupling calculation of the model was based on the principle of effective stress and essentially a one-way seepage-stress coupling. Therefore, it was necessary to carry out the simulation of the excavation step after the completion of the seepage calculation. Tunnel excavation was simulated by passivating the grid group. The length of each excavation was set to 5 cm, and a total of six excavations were performed.

The purpose of the numerical simulation was to verify the accuracy of the physical experiments and to analyze the evolution of percolation channels from a microscopic level. The calculation process was performed under various water pressures. Because of their similar evolution processes, only one case where the water pressure was 0.1 MPa was studied and discussed.

### Seepage evolution process

The evolution process of the pore water pressure isosurface in the numerical model is shown in Fig. 9. In the simulation

process, the seepage-stress coupling calculation was carried out in multiple independent steps. The different colors of the isosurface represent different stages in the calculation process, regardless of the pressure value. The pressure water source was set to the right of the numerical model. Therefore, the value of the right isosurface was larger than that of the left isosurface.

The four photos in Fig. 9 intuitively reflect the magnitude of the seepage pressure at different locations on the same cross-section. The first stage is the initial seepage in the rock mass. The calculation has just been performed, and the pore water pressure only exits on the far-right side of the model. Then, the seepage gradually spreads forward and around, which is consistent with the actual conditions. When the seepage diffuses longitudinally to the middle of the model, the cross-section is filled with pore water pressure, as shown in the second stage. Gravity acts concurrently, causing the pore water pressure in the lower part of the same section to be greater than that in the upper part. If the model is not disturbed by excavation, the seepage continues to be transferred to the front of the model according to the propagation law of the second stage. The third stage is the excavation stage. Due to the excavation and unloading of the filling rock mass, the hydraulic conductivity of the rock mass at the front end of the model becomes stronger. Therefore, in this stage, the middle of the isosurface protrudes forward. At this stage in the physical test, water leakage occurs at the front end of the model. As the excavation continues, the probability of water inrush gradually increases. In the fourth stage, the isosurface in the middle is missing. This is because the seepage surface is set in the central rock mass of the numerical model, not

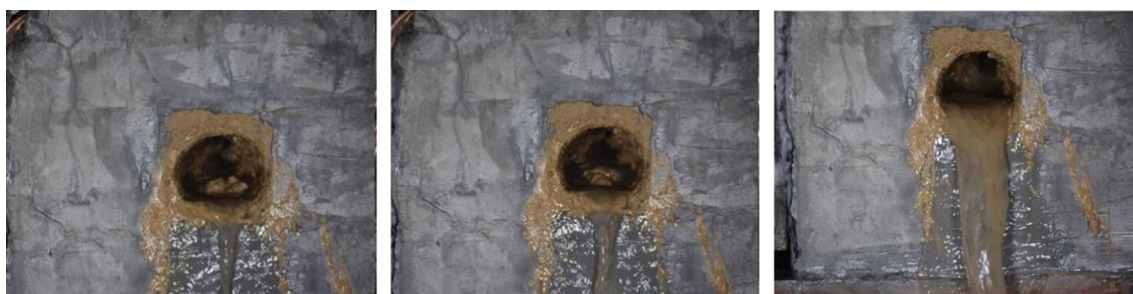


**Fig. 7** Water inrush phenomena in physical experiment



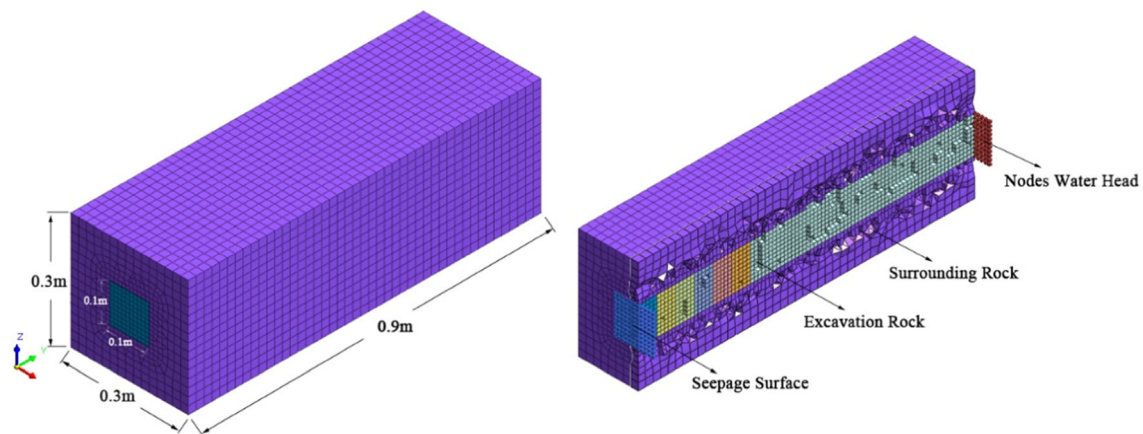


Fig. 8 Numerical model

around. The setting of the seepage surface is mainly to maintain consistency with the physical experiment, ensuring that the water flows out of the filling rock mass.

The variations in the pore water pressure in the initial seepage phase and the excavation phase are shown in Figs. 10 and 11, respectively. It can be seen from Fig. 10 that after the model reaches the initial seepage stability, the first excavation causes a great change in pore water pressure compared with those in the subsequent excavations. The increase in the pore water pressure caused by the first excavation is 6 to 7 times the sum of the increased values caused by the subsequent excavation. According to the distance from the confined water source, monitoring point 5 is the most disturbed, and point 1 is the least disturbed.

### Simulation and experimental verification analysis

For seepage stage and the excavation stage, comparisons of the pore water pressure at each monitoring point of the numerical simulation and the experiment are shown in Figs. 12 and 13, respectively. Monitoring points 1, 3, and 5 in Fig. 13 are selected to verify the consistency of the simulation and experimental results under different excavation distances. Among them, the value of water pressure at monitoring point 5 of the experiment increased sharply when the excavation reaches 0.3 m because water gushing occurs in this step. The results

show that the data error is controlled within 5%. The simulation results are basically consistent with the experimental results, which prove the effectiveness of this simulation for the qualitative analysis of seepage. The simulation can be used as an effective research method to supplement experimental results.

### Discussion

The seepage in the tunnel rock is greatly affected by the first tunnel excavation, and the value of water pressure increases sharply after the first excavation. With the advancement of subsequent excavation, the pore water pressure slowly increases. When the water inrush channel is completely formed, the mutation occurs again. This is because the first excavation breaks the internal balance of the seepage system in the entire tunnel rock mass. As the excavation continues, the seepage channel continues to expand until the entire water inrush channel is formed. The sudden increase in the pore water pressure value at some points is caused by the continuous accumulation of energy in the process of seepage. Most engineers did not pay attention to the damage to the groundwater balance system during the first excavation and could not reasonably monitor the water pressure in the rock mass, which caused many tunnel water inrush disasters.

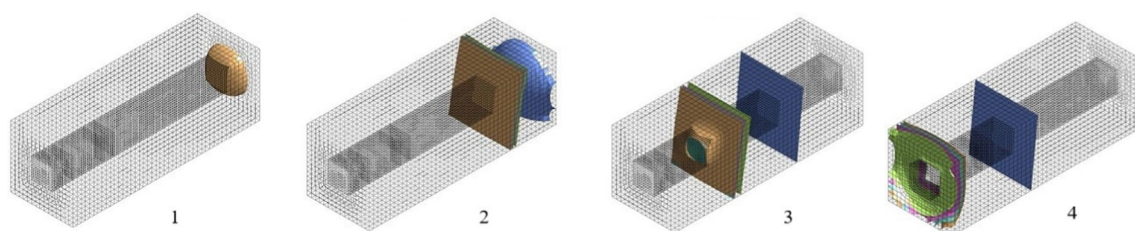


Fig. 9 Iso-surface evolution process of pore water pressure

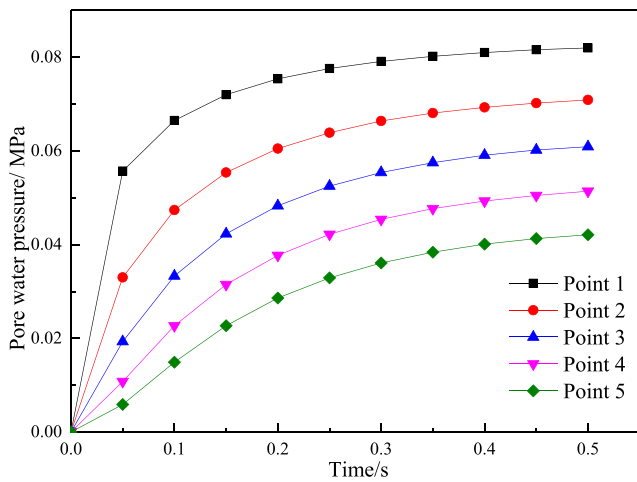


Fig. 10 Pore water pressure during initial seepage

Previous studies have found that the relationship between the confined water head and the thickness of the water-against strata is linear (Huang et al. 2018). This is basically consistent with the results obtained for the experiments in this study. The model is set to a cube to facilitate the loading of the confining pressure during the experiment and simulation, which may be different in actual situations. Due to the limitations of the experimental and model devices, this experiment did not collect and measure the water inrush mixture and the inrush water volume, which will be considered in the future research.

### Conclusions

In this study, a new type of physical test device was applied to carry out tunnel excavation experiments under high ground stress and high water pressure. Based on the numerical software, the corresponding fluid-solid coupling calculations

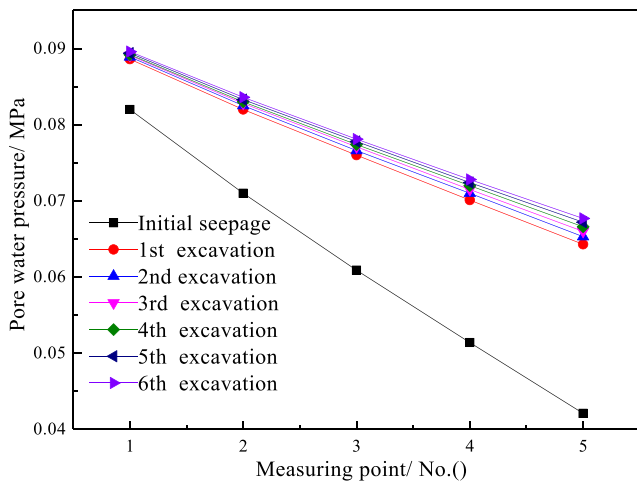


Fig. 11 Pore water pressure during excavation

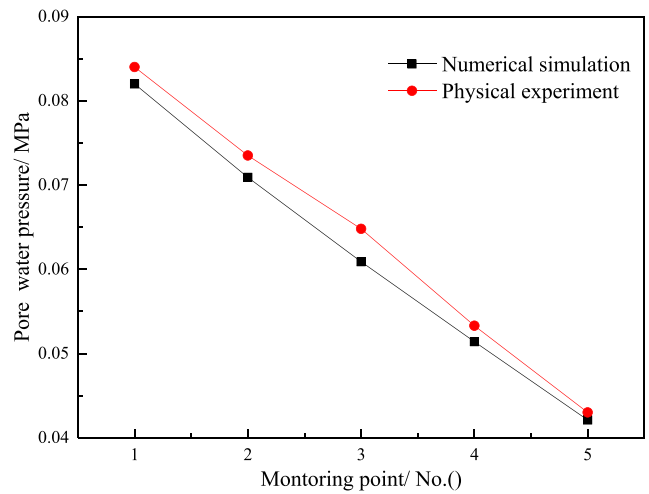


Fig. 12 Comparison of the physical experiment and numerical simulation in the initial seepage stage

were supplemented. Research results that have guiding significance for actual engineering were obtained. The seepage law in the tunnel rock mass under variable water pressure is summarized as follows:

When not disturbed by tunnel excavation, the seepage field in the tunnel rock mass can maintain its own stable state. Moreover, after reaching the initial stability of the seepage, the pore water pressure in the rock mass increases steadily at an extremely slow rate. The pore water pressure is almost proportional to the corresponding water source pressure. In terms of the increase rate of the pore water pressure, that of the rock mass closer to the water source is higher. However, at this stage, large-scale water inrush disasters do not occur.

When the rock mass of the tunnel is disturbed by excavation, the equilibrium state of the seepage field is broken. The original cracks further expand under the disturbance. The pore water pressure in the rock mass increases sharply. The closer the rock mass is to the excavation disturbance surface, the

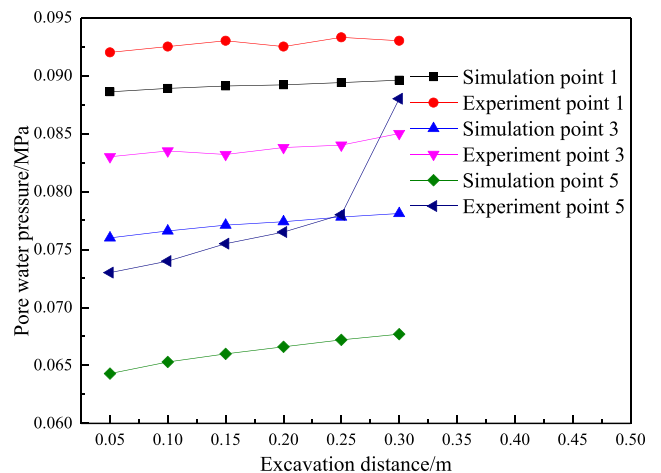


Fig. 13 Comparison of the physical experiment and numerical simulation in the excavation stage

more the internal water pressure increases. This is the opposite of the unexcavated conditions. Therefore, in an actual tunnel project, the groundwater seepage conditions must be clearly identified before the first excavation.

**Funding** Financial supports received from Self-determined Project of State Key Laboratory for Geomechanics and Deep Underground Engineering (Z19010) and the National Natural Science Foundation of China (41572263).

## Compliance with ethical standards

**Conflict of interest** The authors declare that they have no conflict of interest.

## References

- Bukowski P (2011) Water hazard assessment in active shafts in upper Silesian coal basin mines. *Mine Water Environ* 30(4):302–311. <https://doi.org/10.1007/s10230-011-0148-2>
- Chen B, Zhang SC, Li YY et al (2020) Experimental study on water and sand inrush of mining cracks in loose layers with different clay contents. *B Eng Geol Environ*. <https://doi.org/10.1007/s10064-020-01941-5>
- Farhadian H, Nikvar-Hassani A (2019) Water flow into tunnels in discontinuous rock: a short critical review of the analytical solution of the art. *B Eng Geol Environ* 78(5):3833–3849. <https://doi.org/10.1007/s10064-018-1348-9>
- Golian M, Teshnizi ES, Nakhaei M (2018) Prediction of water inflow to mechanized tunnels during tunnel-boring-machine advance using numerical simulation. *Hydrogeol J* 26(8):2827–2851. <https://doi.org/10.1007/s10040-018-1835-x>
- Huang Z, Li SJ, Zhao K et al (2018) Liquid-soild coupling model test to investigate seepage failure mechanism of intact confining rocks of tunnels. *Chines Journal of Basic Science and Engineering* 27(06):1345–1356. (in Chinese). <https://doi.org/10.16058/j.issn.1005-0930.2019.06.014>
- Jiang Q, Yang B, Yan F et al (2020) New method for characterizing the shear damage of natural rock joint based on 3D engraving and 3D scanning. *Int J Geomech* 20(2):06019022. [https://doi.org/10.1061/\(ASCE\)GM.1943-5622.0001575](https://doi.org/10.1061/(ASCE)GM.1943-5622.0001575)
- Jing HW, Yu LY, Su HJ et al (2019) Development and application of catastrophic experiment system for water inrush in surrounding rock of deep tunnels. *Hazard Control in Tunnelling and Underground Engineering* 1(1):102–110 (in Chinese)
- Li SC, Wu J (2019) A multi-factor comprehensive risk assessment method of karst tunnels and its engineering application. *B Eng Geol Environ* 78(3):1761–1776. <https://doi.org/10.1007/s10064-017-1214-1>
- Li SC, Wu J, Xu ZH et al (2016) Numerical analysis of water flow characteristics after inrushing from the tunnel floor in process of karst tunnel excavation. *Geomech Eng* 10(4):471–526
- Li SC, Wang K, Li LP et al (2017) Mechanical mechanism and development trend of water-inrush disasters in karst tunnels. *Chinese Journal of Theoretical & Applied Mechanics* 49(1):22–30. (in Chinese). <https://doi.org/10.6052/0459-1879-16-345>
- Li PF, Liu HC, Zhao Y et al (2018a) A bottom-to-up drainage and water pressure reduction system for railway tunnels. *Tunn. Undergr Sp Tech* 81:296–305. <https://doi.org/10.1016/j.tust.2018.07.027>
- Li PF, Wang F, Long YY et al (2018b) Investigation of steady water inflow into a subsea grouted tunnel. *Tunn. Undergr. Sp Tech* 80:92–102. <https://doi.org/10.1016/j.tust.2018.06.003>
- Li ZY, Wang YC, Olgun G et al (2020) Risk assessment of water inrush caused by karst cave in tunnels based on reliability and GA-BP neural network. *Geomatics, Natural Hazards and Risk* 11(1):1212–1232. <https://doi.org/10.1080/19475705.2020.1785956>
- Lu W (2017) Study on karst water inrush mechanism and treatment method and its engineering applications in tunnels. Dissertation, Shandong University
- Pan DD, Li SC, Xu ZH et al (2019) Experimental and numerical study of the water inrush mechanisms of underground tunnels due to the proximity of a water-filled karst cavern. *B Eng Geol Environ* 78(8):6207–6219. <https://doi.org/10.1007/s10064-019-01491-5>
- Wang YC, Yin X, Jing HW et al (2016) A novel cloud model for risk analysis of water inrush in karst tunnels. *Environ Earth Sci* 75(22):1–13. <https://doi.org/10.1007/s12665-016-6260-7>
- Wang YC, Jing HW, Yu LY et al (2017) Set pair analysis for risk assessment of water inrush in karst tunnels. *B Eng Geol Environ* 76(3):1199–1207. <https://doi.org/10.1007/s10064-016-0918-y>
- Wang J, Li SC, Li LP et al (2019a) Attribute recognition model for risk assessment of water inrush. *B Eng Geol Environ* 78(2):1057–1071. <https://doi.org/10.1007/s10064-017-1159-4>
- Wang XT, Li SC, Xu ZH et al (2019b) Risk assessment of water inrush in karst tunnels excavation based on normal cloud model. *B Eng Geol Environ* 78(5):3783–3798. <https://doi.org/10.1007/s10064-018-1294-6>
- Wang YC, Olgun CG, Wang LB et al (2019c) Risk assessment of water inrush in karst tunnels based on the ideal point method. *Pol J Environ Stud* 28(9):901–911. <https://doi.org/10.15244/pjoes/85199>
- Wang YC, Geng F, Yang SQ et al (2019d) Numerical simulation of particle migration from crushed sandstones during groundwater inrush. *J Hazard Mater* 362:327–335. <https://doi.org/10.1016/j.jhazmat.2018.09.011>
- Wang YC, Chen F, Yin X et al (2019e) Study on the risk assessment of water inrush in karst tunnels based on intuitionistic fuzzy theory. *Geomatics, Natural Hazards and Risk* 10(1):1070–1083. <https://doi.org/10.1080/19475705.2018.1564374>
- Wu XJ (2017) Study on mechanism of seepage and water-inrush from filled karst conduit in tunnel. Dissertation, China University of Mining and Technology
- Wu J, Li SC, Xu ZH et al (2019a) Determination of required rock thickness to resist water and mud inrush from karst caves under earthquake action. *Tunn Undergr Sp Tech* 85:43–55. <https://doi.org/10.1016/j.tust.2018.11.048>
- Wu J, Li SC, Xu ZH (2019b) Numerical analysis of gas-liquid two-phase flow after water inrush from the working face during tunnel excavation in a karst region. *B Eng Geol Environ* 78(4):2973–3010. <https://doi.org/10.1007/s10064-018-1312-8>
- Yang WM, Fang ZD, Wang H et al (2019) Analysis on water inrush process of tunnel with large buried depth and high water pressure. *Processes* 7(3). <https://doi.org/10.3390/pr7030134>
- Zhang JQ, Li SC, Zhang QS et al (2018) Experimental research on destruction characteristics of tunnel mud inrush using transparent soils. *China Journal of Highway and Transport* 31(10):177–189 (in Chinese)
- Zhang JQ, Li SC, Zhang QS et al (2019) Mud inrush flow mechanisms: a case study in a water-rich fault tunnel. *B Eng Geol Environ* 78(8):6267–6283. <https://doi.org/10.1007/s10064-019-01508-z>
- Zhang Y, Zhang DL, Fang Q et al (2020) Analytical solutions of non-Darcy seepage of grouted subsea tunnels. *Tunn Undergr Sp Tech*:96. <https://doi.org/10.1016/j.tust.2019.103182>
- Zhao N, Wang YC, Meng B et al (2018) Numerical simulation on the seepage properties of soil-rock mixture. *Adv Mater Sci Eng* 2018. <https://doi.org/10.1155/2018/1859319>
- Zhou Y, Li SC, Li LP et al (2015) 3D fluid-solid coupled model test on water-inrush in tunnel due to seepage from filled karst conduit. *Chin J Rock Mech Eng* 34(9):1739–1749. <https://doi.org/10.13722/j.cnki.jrme.2014.1393>
- Zhu HT (2010) Study on the rule of water pressure upon lining and treatment technique upon Qiyueshan karst. Dissertation, Beijing Jiaotong University